



---

1 **Insight into the in-cloud formation of oxalate based on in situ measurement**  
2 **by single particle mass spectrometry**

3

4 Guohua Zhang<sup>1</sup>, Qin hao Lin<sup>1,2</sup>, Long Peng<sup>1,2</sup>, Yuxiang Yang<sup>1,2</sup>, Yuzhen Fu<sup>1,2</sup>, Xinhui Bi<sup>1,\*</sup>, Mei

5 Li<sup>3</sup>, Duohong Chen<sup>4</sup>, Jianxin Chen<sup>5</sup>, Zhang Cai<sup>6</sup>, Xinming Wang<sup>1</sup>, Ping'an Peng<sup>1</sup>, Guoying

6 Sheng<sup>1</sup>, Zhen Zhou<sup>3</sup>

7

8 <sup>1</sup> State Key Laboratory of Organic Geochemistry and Guangdong Key Laboratory of

9 Environmental Resources Utilization and Protection, Guangzhou Institute of Geochemistry,

10 Chinese Academy of Sciences, Guangzhou 510640, PR China

11 <sup>2</sup>University of Chinese Academy of Sciences, Beijing 100039, PR China

12 <sup>3</sup> Atmospheric Environment Institute of Safety and Pollution Control, Jinan University,

13 Guangzhou 510632, PR China

14 <sup>4</sup> State Environmental Protection Key Laboratory of Regional Air Quality Monitoring,

15 Guangdong Environmental Monitoring Center, Guangzhou 510308, PR China

16 <sup>5</sup> Shaoguan Environmental Monitoring Center, Shaoguan 512026, PR China

17 <sup>6</sup> John and Willie Leone Family Department of Energy and Mineral Engineering, The

18 Pennsylvania State University, University Park, PA 16802, USA

19

20 Correspondence should be addressed to Xinhui Bi ([bixh@gig.ac.cn](mailto:bixh@gig.ac.cn))



---

21 **Highlights**

22 ● Single particle mixing state of oxalate in the cloud-free, residual, and interstitial particles

23 was first reported.

24 ● Direct observational evidence showed the enhanced formation of oxalate in the cloud

25 residual and interstitial particles.

26 ● Chemically segregated formation of oxalate was observed depending on the oxidized

27 organics associated with aged biomass burning particles.

28 ● Glyoxylate served as an important intermediate for the formation of oxalate in the

29 troposphere of southern China.

30



---

## 31 Abstract

32 While ground-based works suggest the significance of in-cloud production (or aqueous  
33 formation) to oxalate, direct evidence is rare. With the in situ measurements performed at a  
34 remote mountain site (1690 m a.s.l.) in southern China, we first reported the size-resolved  
35 mixing state of oxalate in the cloud droplet residual (cloud RES), the cloud interstitial (cloud  
36 INT), and ambient (cloud-free) particles by single particle mass spectrometry. The results  
37 support the growing evidence that in-cloud aqueous reactions promote the formation of oxalate,  
38 with ~15% of the cloud RES and cloud INT particles containing oxalate, in contrast to only ~5%  
39 of the cloud-free particles. Furthermore, individual particle analysis provides unique insight  
40 into the formation and evolution of oxalate during in-cloud processing. Oxalate was  
41 predominantly (>70% in number) internally mixed with the aged biomass burning particles,  
42 highlighting the impact of biomass burning on the formation of oxalate. In contrast, oxalate was  
43 underrepresented in aged elemental carbon particles, although they represented the largest  
44 fraction of the detected particles. It can be interpreted by the individual particle mixing state  
45 that the aged biomass burning particles contained an abundance of organic components serving  
46 as precursors for oxalate. Through the analysis of the relationship between oxalate and organic  
47 acid ions ( $-45[\text{HCO}_2]^-$ ,  $-59[\text{CH}_3\text{CO}_2]^-$ ,  $-71[\text{C}_2\text{H}_3\text{CO}_2]^-$ ,  $-73[\text{C}_2\text{HO}_3]^-$ ), the results show that in-  
48 cloud aqueous reaction dramatically improved the conversion of organic acids to oxalate. The  
49 abundance of glyoxylate associated with the aged biomass burning particles is the controlling  
50 factor for the in-cloud production of oxalate. Since only limited information on oxalate is



---

51 available in the free troposphere, the results also provide an important reference for future

52 understanding of the abundance, evolution and climate impacts of oxalate.

53

54 **Keywords:** oxalate, individual particles, cloud droplet residues, mixing state, organic acids,

55 biomass burning



---

## 56 **1 Introduction**

57 In-cloud processing represents a large uncertainty in understanding the evolution and  
58 impact of secondary organic aerosols (SOA) on both environment and climate (Ervens, 2015;  
59 Ervens et al., 2011; Herrmann et al., 2015). Dicarboxylic acids significantly contribute to  
60 SOA, aerosol acidity and hygroscopicity, and thus play an important role in atmospheric  
61 chemistry and cloud condensation nuclei (CCN) (Ervens et al., 2011; Furukawa and  
62 Takahashi, 2011; Sorooshian et al., 2013). Oxalic acid is globally the most abundant  
63 dicarboxylic acid (Kawamura and Bikkina, 2016; Ho et al., 2010; Mochida et al., 2007),  
64 accounting for as high as 5% of water soluble organic compounds downwind of the mainland  
65 China (Feng et al., 2012; Kawamura and Bikkina, 2016). In addition, oxalate has great  
66 impact on the solubility, photochemistry and bioavailability of transition metals in aerosols  
67 (Ito and Shi, 2016; Johnson and Meskhidze, 2013).

68 Although there are primary sources, such as combustion of coal/biomass and biogenic  
69 origins, oxalate is generally regarded as an oxidation product of malonate and glyoxylate,  
70 precursors of which include glyoxal, methylglyoxal, glycolic acid, pyruvic acid, acetic acid  
71 and so on (Carlton et al., 2006; Myriokefalitakis et al., 2011; Kawamura and Bikkina, 2016).  
72 Large multifunctional compounds might also be important for the formation of oxalate  
73 (Carlton et al., 2007). The formation pathways mainly include photochemical oxidation  
74 followed by partitioning onto particulate phase and in-cloud aqueous formation (Yu et al.,  
75 2005; Guo et al., 2016; Sullivan et al., 2007). The in-cloud aqueous pathway is generally  
76 proposed as the dominant pathway based on the similar pattern between both size



---

77 distribution and concentration of oxalate and sulfate (Yu et al., 2005; Huang et al., 2006;  
78 Laongsri and Harrison, 2013). However, Zhou et al. (2015) argued that only 16% of oxalate  
79 could be attributed to in-cloud production, despite of its robust correlation with sulfate.  
80 Photochemical oxidation could account for ~80% of oxalate in air mass influenced by  
81 biomass burning (Kundu et al., 2010). More direct evidences are needed to better evaluate  
82 the formation and behavior of oxalate during in-cloud processing. Through aircraft  
83 measurements, Sorooshian et al. (2006) revealed higher concentration of oxalate in cloud  
84 droplet residual (cloud RES) particles, rather than in cloud-free atmospheric particles over  
85 Ohio, USA. Similarly, elevated oxalate levels due to in-cloud processing were observed  
86 above coastal USA (Crahan et al., 2004), and Gulf of Mexico (Sorooshian et al., 2007a;  
87 Wonaschuetz et al., 2012; Sorooshian et al., 2007b). Recently, an aircraft measurement also  
88 provided an evidence on the important role of in-cloud production of oxalate from the near  
89 surface to the lower free troposphere (i.e., ~2 km) over inland China (Zhang et al., 2016).  
90 All of these in-situ observations were based on bulk particles analysis, and thus might miss  
91 some valuable information on the mixing state of oxalate, which is demonstrated to be  
92 significant for evaluating the life time and environmental impact of oxalate (Sullivan et al.,  
93 2007; Zhou et al., 2015). Information on oxalate in the atmosphere associated with cloud  
94 formation is still rare, far from enough for thoroughly understanding its distribution, sources,  
95 formation, evolution and environmental impact (Kawamura et al., 2013; Meng et al., 2014;  
96 Meng et al., 2013).



97           Single particle mass spectrometry (SPMS) has been commonly applied to obtain mixing  
98 state of individual oxalate-containing particles, which is essential for their atmospheric  
99 behaviors and environment impacts (Sullivan et al., 2007). Based on SPMS, oxalate was  
100 found to be extensively internally mixed with sulfate in the Arctic boundary layer (Hara et  
101 al., 2002). Similarly, the relative contributions of in-cloud processing, heterogeneous  
102 reactions and biomass burning to oxalate in Shanghai was investigated (Yang et al., 2009).  
103 Sullivan et al. (2007) demonstrated the significant contribution of photochemical formation  
104 to oxalate followed by partitioning onto the dust and sea-salt particles. Zhou et al. (2015)  
105 proposed that oxalate was readily photo-degraded in a form of oxalate-Fe complex in Hong  
106 Kong. However, such studies have not been conducted to investigate the in-cloud formation  
107 of oxalate. Investigation on the single particle mixing state of cloud/fog RES and interstitial  
108 (cloud INT) particles would provide unique insight into the formation and aging processes  
109 of aerosol compositions (Zhang et al., 2012; Bi et al., 2016; Li et al., 2011b; Pratt et al.,  
110 2010).

111           To better understand the in-cloud aqueous formation of oxalate, we investigated  
112 individual oxalate-containing particles at a high-altitude mountain site, representative of the  
113 free troposphere in southern China. Using a single particle aerosol mass spectrometer  
114 (SPAMS), the size-resolved mixing state of cloud-free, cloud RES and cloud INT oxalate-  
115 containing particles were investigated. This paper reported data supporting the in-cloud  
116 production of oxalate, and also discussed the influence of mixing state on the in-cloud  
117 production.



118

119 **2 Methods**120 **2.1 Cloud observation**

121 Measurements of the cloud-free, cloud RES, and cloud INT particles were performed at  
122 the Nanling national background site (24°41'56"N, 112°53'56"E, 1690 m a.s.l.) in southern  
123 China during 16-26 January 2016. Air masses from the southwestern continental and marine  
124 areas dominated over the sampling period, bringing relatively warmer and wetter air masses  
125 that benefited cloud formation (Lin et al., 2017), based on the back-trajectory analysis  
126 (HYSPLIT 4.9, available at <http://ready.arl.noaa.gov/HYSPLIT.php>) by Air Resources Lab  
127 (Draxler and Rolph, 2012). The air masses from northern areas, associated with cool dry  
128 airstreams, arrived during 18 and 23-24 January, resulted in a decrease in both temperature  
129 and relative humidity. Cloud events were characterized by a sudden drop in visibility (to <  
130 5 km) and a sharp increase in relative humidity (> 95%) (Lin et al., 2017). In this study, three  
131 long lasting (more than 12 hours) cloud events (Fig. 1), noted as cloud I, cloud II, and cloud  
132 III, were identified. The visibility were generally lower than 1 km during the cloud events.

133 Aerosols were introduced into the instruments through two parallel sampling inlets. The  
134 first one was a ground-based counterflow virtual impactor (GCVI) (Model 1205, Brechtel  
135 Mfg. Inc., USA), applied to collect the cloud RES particles with a diameter greater than 8  
136  $\mu\text{m}$ . The GCVI employed a compact wind tunnel upstream of the CVI inlet (Model 1204)  
137 to accelerate cloud droplets in the CVI inlet tip (Shingler et al., 2012). Upstream of the CVI  
138 sampling tip, only droplets exceeding a certain controllable size (or cut size) could pass





---

139 through the counterflow and enter the evaporation chamber (with an air flow temperature at  
140 40 °C), where the droplets were dried, leaving the cloud RES particles that are capable of  
141 acting as CCN. A 15 L/min sample flow was provided to the downstream instruments. The  
142 enhancement factor for particles concentration collected by GCVI was 5.25, corresponding  
143 to the designation of the CVI. The detailed characterization and validation of the CVI  
144 sampling efficiency could be found elsewhere (Shingler et al., 2012). The flow rates of the  
145 whole GCVI system were validated before measurements, and were also automatically  
146 monitored throughout the operation. A test on the cloud-free air showed that the average  
147 particles number concentration sampled by the GCVI was  $\sim 1 \text{ cm}^{-3}$ , in contrast to  $\sim 2000 \text{ cm}^{-3}$   
148  $\text{cm}^{-3}$  in ambient air. The testing demonstrates that the influence of background particles on the  
149 collection of the cloud RES particles could be negligible, further validating the performance  
150 of the GCVI. In the present study, the average number concentration of the cloud RES  
151 particles sampled during the cloud events was  $\sim 250 \text{ cm}^{-3}$  (Lin et al., 2017). The other one  
152 ambient ( $\text{PM}_{2.5}$ ) sampling inlet was used to deliver cloud-free or cloud INT particles.

153

## 154 2.2 Instrumentation

155 A SPAMS (Hexin Analytical Instrument Co., Ltd., Guangzhou, China), an  
156 Aethalometer (AE-33, Magee Scientific Inc.), and a scanning mobility particle sizer (SMPS;  
157 MSP Cooperation) were conducted to characterize the physical and chemical properties of  
158 the sampled particles. During cloud I and cloud II, the instruments were connected  
159 downstream the GCVI. During cloud III, cloud RES and cloud INT particles were alternately



---

160 sampled with an interval of ~1 h. During the cloud-free periods, these instruments were  
161 connected to the ambient inlet in order to measure the cloud-free particles. The presented  
162 results focused on the chemical composition and mixing state of the oxalate-containing  
163 particles detected by the SPAMS. Therefore, details for other instruments were not provided  
164 herein.

165

### 166 **2.3 Detection and classification of oxalate-containing particles**

167 The vacuum aerodynamic diameter ( $d_{va}$ ) and mass spectral information for individual  
168 particles could be obtained by the SPAMS (Li et al., 2011a). A brief description on  
169 performance of the SPAMS can be found in the Supplement. Assuming Poisson distribution,  
170 standard errors for the number fraction (Nf) of particles were estimated (Pratt et al., 2010),  
171 since the particles were randomly detected by the SPAMS. Oxalate-containing particles are  
172 identified as particles with ion peak at  $m/z$  -89 (Sullivan and Prather, 2007; Zauscher et al.,  
173 2013), and their number-based mass spectra is shown in Fig. S1 in the Supplement.  
174 Approximate 6000 particles were identified as oxalate-containing particles, accounting for  
175  $8.1 \pm 0.1\%$  of the total detected particles in the size range of 100-1600 nm. They were  
176 clustered by an adaptive resonance theory-based neural network algorithm (ART-2a), based  
177 on the presence and intensity of ion peaks (Song et al., 1999). Eight types with distinct mass  
178 spectral characteristics (Fig. S2) were obtained for further analysis. More detail information  
179 on all the observed particle types could be found elsewhere (Lin et al., 2017).

180



---

## 181 3 Results and Discussion

### 182 3.1 Direct observational evidence for in-cloud production of oxalate

183 The Nfs of the oxalate-containing particles relative to all the cloud-free, cloud RES, and  
184 cloud INT particles were  $5.0 \pm 0.1\%$ ,  $14.4 \pm 0.2\%$ , and  $13.4 \pm 1.1\%$ , respectively (Table 1).

185 The Nfs of the oxalate-containing particles varied from near zero in the cloud-free particles  
186 to ~80% in the cloud RES or cloud INT particles (Figure 1). Consistently, the average  
187 relative peak area (RPA) of oxalate in the cloud RES and cloud INT particles suppressed by  
188 a factor of ~8 that in the cloud-free particles. Defined as fractional peak area of each m/z  
189 relative to the sum of peak areas in a mass spectrum, RPA could represent the relative  
190 amount of a species on a particle (Jeong et al., 2011; Healy et al., 2013). At ground level in  
191 China, oxalate was found in ~3% of total particles in Shanghai (Yang et al., 2009) and the  
192 PRD region (Cheng et al., 2017), respectively. Relatively higher fraction of oxalate-  
193 containing particles in this study might reflect the importance of atmospheric ageing during  
194 long-range transport for the formation of oxalate at the high mountain site of southern China.

195 Analogous Nfs of the oxalate-containing particles in the cloud RES and cloud INT  
196 particles suggest the similar formation mechanism of oxalate in cloud droplets and interstitial  
197 particles, although Dall'Osto et al. (2009) indicated that difference might exist for secondary  
198 compounds formation between fog droplets and INT particles. The Nfs of the oxalate-  
199 containing particles in the cloud-free, cloud RES, and cloud INT particles versus  $d_{va}$  are  
200 displayed in Fig. 2. Oxalate-containing particles had higher Nfs in the smaller cloud-free  
201 particles, indicative of primary emission or photochemical production followed by



---

202 condensation (Zauscher et al., 2013). On the contrary, the Nfs of the oxalate-containing  
203 particles in the cloud RES and cloud INT particles increased with increasing  $d_{va}$ , showing a  
204 distinctly different pattern. It indicates that in-cloud aqueous reaction grows the cloud RES  
205 and cloud INT oxalate-containing particles with addition of secondary compositions  
206 (Schroder et al., 2015). It is further supported by the unscaled number size distribution of  
207 the cloud-free, cloud RES, and cloud INT oxalate-containing particles (Fig. S3), with  $d_{va}$   
208 peaking at around 0.5, 0.8, and 0.7  $\mu\text{m}$ , respectively.

209 It is further shown that the enhanced Nfs of the oxalate-containing particles was not  
210 likely due to the influence of air mass. Firstly, the Nfs of the cloud-free oxalate-containing  
211 particles were generally low (< 10%) over the sampling period (Fig. 1 and Fig. S4), reflecting  
212 a background level of oxalate. Secondly, the Nfs and the RPAs of the cloud RES oxalate-  
213 containing particles exclusively sharply increased when RH was larger than 95% (Fig. S4).  
214 Significant enrichment of oxalate in the cloud RES particles demonstrates the importance of  
215 in-cloud aqueous reactions in the formation of oxalate (Sorooshian et al., 2006). Overall,  
216 these results provide direct evidences that the in-cloud aqueous processing is the dominant  
217 mechanism for oxalate in this study. More details on the formation mechanism and the  
218 dominant influence factors would be discussed in the following text.

219

### 220 **3.2 Predominant contribution of biomass/biofuel burning to oxalate**

221 Number fractions of the major ion peaks associated with the oxalate-containing particles  
222 were compared to those with all the detected particles, as shown in Fig. 3. Detailed



223 information on the Nfs of all the detected ion peaks in the oxalate-containing particles could  
224 be found in Fig. S1. Potassium, with intense peak (peak area > 1000) at  $m/z$  39 Da, is  
225 ubiquitously (~90%) associated with the oxalate-containing particles. It is attributed to  
226 highly sensitive of potassium to the desorption laser in the SPAMS, although  $m/z$  39 Da may  
227 also be appointed to  $39[\text{C}_3\text{H}_3]^+$  (Silva et al., 1999). Sulfate ( $-97[\text{HSO}_4]^-$ , 96%) and nitrate ( $-$   
228  $62[\text{HNO}_3]^-$ , 88%) were the dominant secondary inorganic species associated with the  
229 oxalate-containing particles. Other major ion peaks were ammonium ( $18[\text{NH}_4]^+$ , 47%),  
230 organic nitrogen ( $-26[\text{CN}]^-$ , 76%), and oxidized organics (i.e.,  $m/z$  -45, -59, -71, and -73)  
231 with the Nfs ranging from 17% to 57%. These oxidized organics were commonly found in  
232 aged biomass burning particles, regarded as organic acids (OAs). Their RPAs increased with  
233 increasing particle sizes (Fig. S5), indicative of secondary origins (Zauscher et al., 2013).  
234 Furthermore, these OAs, most likely assigned to be formate at  $m/z$   $-45[\text{HCO}_2]^-$ , acetate at  
235  $m/z$   $-59[\text{CH}_3\text{CO}_2]^-$ , methylglyoxal or acrylate at  $m/z$   $-71[\text{C}_2\text{H}_3\text{CO}_2]^-$ , and glyoxylate at  $m/z$   
236  $-73[\text{C}_2\text{HO}_3]^-$  (Zauscher et al., 2013), tracked each other temporally (Table S1), supporting  
237 their similar formation mechanisms. Other OAs with minor fraction (~10%) were also  
238 detected to be associated with the oxalate-containing particles, such as  $m/z$  -87, -103, and -  
239 117 Da due to pyruvate, malonate, and succinate, respectively. OAs could be formed through  
240 oxidation of volatile organic compounds in biomass burning plume (Zauscher et al., 2013).  
241 Continuous evolution of primary organics to highly oxidized organics is widely observed for  
242 biomass burning particles (Zhou et al., 2017; Cubison et al., 2011). The extensive presence  
243 of potassium, OAs, and organic nitrogen in the oxalate-containing particles reflects the



---

244 substantial contribution of biomass burning to the observed oxalate (Zauscher et al., 2013;  
245 Pratt et al., 2010). The oxalate-containing particles observed herein likely represented aged  
246 biomass burning particles with enhanced aliphatic acids (Paglione et al., 2014). Significant  
247 correlations between these OAs were observed in aged biomass burning particles (Zauscher  
248 et al., 2013) and also cloud water samples (Sorooshian et al., 2013). Hence, it is expected  
249 that the Nfs of these OAs were obviously larger in the oxalate-containing particles, rather  
250 than those in the other detected particles (Fig. 3).

251 The contribution of biomass burning to the observed oxalate could also be reflected by  
252 the overwhelming potassium-rich (K-rich) particles (Table 1 and Fig. S2), regarded as aged  
253 biomass burning particles herein (Bi et al., 2011; Pratt et al., 2010; Zauscher et al., 2013).  
254 Following emission, biomass burning particles become enriched in sulfate, nitrate, and OAs  
255 as ageing processes (Reid et al., 2005). It can be seen in Fig. 4 that  $75.1 \pm 1.5\%$  of oxalate  
256 was associated with the K-rich particles, although they only accounted for  $36.0 \pm 0.3\%$  of  
257 all the detected particles (Lin et al., 2017). Only  $4.0 \pm 0.4\%$  of oxalate was associated with  
258 the aged elemental carbon (EC) particles although they were the dominant fraction ( $45.0 \pm$   
259  $0.3\%$ ) of all the detected particles, reflecting an external mixing state. Enhancement of  
260 oxalate in the K-rich particles supports the favorable formation of oxalate in aged biomass  
261 burning particles. Such a high fraction (i.e.,  $75.1 \pm 1.5\%$ ) in the present study indicates a  
262 substantial contribution from secondary processing of biomass burning particles, as  
263 discussed above. The result is consistent with previous studies that observed abundance of  
264 oxalate substantially influenced by aged biomass burning particles (Gao et al., 2003;



265 Deshmukh et al., 2016; Yang et al., 2014; Zhou et al., 2015). Primary emission from biomass  
266 burning contributes only a minor fraction to the observed oxalate in the atmosphere in China  
267 (Meng et al., 2013; Yang et al., 2009). Direct observation also supports the absence of  
268 oxalate in primary biomass burning particles (Silva et al., 1999; Huo et al., 2016).

269 As shown in Fig. 4, ~10% of oxalate was associated with Fe-rich particles, second only  
270 to the K-rich particles. Regarding that the Fe-rich particles only accounted for  $2.5 \pm 0.4\%$  of  
271 all the detected particles (Lin et al., 2017), it might reflect that the Fe facilitated the formation  
272 of oxalate. Fenton reactions involving iron can produced more oxidants (e.g.,  $\bullet\text{OH}$ )  
273 (Herrmann et al., 2015; Nguyen et al., 2013), which is an important factor for the formation  
274 of oxalate (Ervens et al., 2014). Likewise, the highest fraction ( $> 30\%$ ) of oxalate was found  
275 to be internally mixed with metal-containing (e.g., iron, zinc, copper) particles in the Pearl  
276 River Delta region (Cheng et al., 2017). Oxalate was also found to be slightly enriched in  
277 amine-containing particles, which is most probably attributed to the enhanced partition of  
278 amine to wet aerosols (Zhang et al., 2012; Rehbein et al., 2011).

279

### 280 **3.3 Pathway for in-cloud formation of oxalate in aged biomass burning particles**

281 As shown in Table 1,  $> 70\%$  of oxalate by number was associated with the aged biomass  
282 burning particles. It is also noted that ~10% of the cloud-free K-rich particles contained  
283 oxalate, while the fraction increased to  $> 20\%$  in the cloud INT and cloud RES K-rich  
284 particles. This is not likely due to the preferential activation of the K-rich particles, since the  
285 Nfs of oxalate associated with the K-rich particles is similar (70-76%) for the cloud-free,



---

286 cloud RES, and cloud INT particles (Fig. S6). Therefore, the favorable formation of oxalate  
287 in the K-rich particles is most probably attributed to the enhanced organic precursors, as  
288 discussed in the following.

289 The major OAs were predominantly associated with the oxalate-containing particles  
290 (Fig. 3) and also the K-rich particles (Table S2). Furthermore, significant correlations ( $p <$   
291 0.01) were found for the temporal profiles of the Nfs of the OAs and that of the oxalate-  
292 containing particles, particularly, for the cloud RES particles (Table S1). The highest  
293 correlation was found between the oxalate-containing particles and the glyoxylate-  
294 containing particles in the Nf and the RPA (Fig. 5). The correlations were significantly  
295 stronger for the cloud RES and cloud INT particles rather than for the cloud-free particles,  
296 suggesting the in-cloud production from glyoxylate as an important pathway for oxalate. It  
297 should further confirm the assignment of  $m/z$  -73 to glyoxylate, regarded as one of the  
298 primary intermediates contributing to formation of oxalate (Carlton et al., 2006;  
299 Myriokefalitakis et al., 2011). Miyazaki et al. (2009) suggested that secondary production of  
300 oxalate probably in aqueous phase is important via the oxidation of both longer-chain diacids  
301 and glyoxylate, and would be enhanced in biomass burning influenced particles. To our  
302 knowledge, it is the first report on the direct link and the internally mixing state between  
303 glyoxylate and oxalate during in-cloud processing with high time resolution. Additionally,  
304 the linear regression slopes between glyoxylate and oxalate for the cloud RES and cloud INT  
305 particles were also higher than that for the cloud-free particles (Fig. 5), which also supports  
306 the more effective production of oxalate in cloud.





307 We further analyzed the relative fraction of the peaks areas of oxalate, glyoxylate, and  
308 OAs in oxalate-containing particles during the cloud-free periods and cloud events (Fig. 6).  
309 It can be seen that the dots distribute close to the OAs during cloud-free periods, whereas  
310 they distribute towards oxalate during cloud events. This distribution indicates that the OAs  
311 were the dominant composition relative to oxalate and glyoxylate in the cloud-free oxalate-  
312 containing particles, whereas oxalate became more important in the cloud RES and cloud  
313 INT oxalate-containing particles. The different pattern is attributable to the conversion of  
314 the OAs to oxalate as a result of in-cloud aqueous reactions. It is also supported by the  
315 variations of the Nfs of the major OAs in the cloud-free, cloud RES, and cloud INT particles,  
316 respectively (Fig. S7). A substantial decrease (~50% on average) is found for the Nfs of the  
317 OAs associated with the oxalate-containing particles, from the cloud-free particles to the  
318 cloud RES and cloud INT particles. On the other hand, the Nfs of the OAs in all the detected  
319 particles did not show an obvious decrease. The conversion of the OAs to oxalate during in-  
320 cloud processing is consistent with the observation that oxalate increased as the droplets  
321 evaporated, while acetate, glyoxylate, and malonate decreased (Sorooshian et al., 2007b).

322 Most of previous studies considered that glyoxylate is dominantly produced from  
323 aqueous oxidation of glyoxal or glycolic acid, depending on volatile organic compounds  
324 (Sorooshian et al., 2006; Sorooshian et al., 2007b; Ervens et al., 2004). Aqueous phase  
325 reaction promotes the production of oxalate through increasing the partitioning of gases into  
326 droplets (Sorooshian et al., 2007a). If this pathway dominated in this study, glyoxylate and  
327 oxalate should be evenly distributed in all the particle types, which is inconsistent with our



---

328 observation that they were predominantly associated with the aged biomass burning particles  
329 (Fig. 3). It indicates that a certain amount of glyoxylate should be directly produced in cloud  
330 from the organics formed before the cloud events and associated with aged biomass burning  
331 particles. Aqueous-phase processing of biomass-burning emissions was demonstrated to be  
332 a substantial contributor to the SOA (Gilardoni et al., 2016). Existing models typically treat  
333 cloud droplets as a well-mixed bulk aqueous phase (McNeill, 2015), and initialize the  
334 particle composition as pure ammonium sulfate (Ervens et al., 2004; Sorooshian et al., 2006).  
335 Our results suggest that a particle type based model with detailed chemical mixing state is  
336 required for further understanding on the modification of particle properties by in-cloud  
337 processing in the troposphere.

338

### 339 **3.4 Case study for the influence of air mass on the formation of oxalate**

340 Cloud II represented a relatively more polluted condition, with  $PM_{2.5}$  around  $200 \text{ ng m}^{-3}$   
341  $^3$ , ~4 times those during cloud I and III. Air mass analysis showed that cloud II was strongly  
342 influenced by northeastern air mass, contrasting to the southwestern air mass during cloud I  
343 and III (Lin et al., 2017). Figure 7 compares the respective Nfs of the K-rich, oxalate-  
344 containing, and glyoxylate-containing particles during the three cloud events. The K-rich  
345 particles were found to contribute ~25% of the cloud RES particles during cloud II, which  
346 was significantly lower than its contribution (~50%) during cloud I and III. Similarly, Nf of  
347 the glyoxylate-containing particles during cloud II was significantly lower, which is also  
348 similar for other oxidized organics (Table S3). Since oxalate was predominantly associated



---

349 with the aged biomass burning particles, Nf of the oxalate-containing particles shares a  
350 similarly trend. This is because the in-cloud production of oxalate on the aged biomass  
351 burning particles is dominantly controlled by the glyoxylate. It is also supported by higher  
352 correlation between the Nfs of oxalate-containing and glyoxylate-containing particles,  
353 relative to that between the Nfs of oxalate-containing particles and the aged biomass burning  
354 particles (Table S1). The result suggests that aged biomass burning particles from  
355 northeastern air mass contained less amount of oxidized organics for the formation of oxalate.  
356 We also note that short cloud processing time should not be the reason for the lower Nf of  
357 oxalate-containing particles during cloud II. As can be seen in Fig. 1, the Nf of oxalate-  
358 containing particles increased to 20% within several hours during cloud I and III.

359

#### 360 **4 Conclusions**

361 Individual particle mixing state of oxalate in the cloud-free, cloud RES and cloud INT  
362 particles obtained at a remote mountain site allows for the investigation of formation and  
363 evolution of oxalate. Our results show significant enhancement of oxalate-containing  
364 particles in the cloud RES and cloud INT particles, rather than in the cloud-free particles,  
365 providing first direct observational evidence for the in-cloud production of oxalate in the  
366 troposphere in China, and strengthening the growing evidence that aqueous-phase chemistry  
367 is the predominant formation mechanism for oxalate. The influence of biomass burning on  
368 the formation of oxalate was also highlighted, with predominant fraction (> 70%) of oxalate  
369 internally mixed with aged biomass burning particles. Formation of oxalate is highly



---

370 dependent on the abundance of organic acids strongly associated with the aged biomass  
371 burning particles, with glyoxylate as an important intermediate. In-cloud chemically  
372 segregated production of oxalate would lead to a substantial change of the biomass burning  
373 particles after cloud evaporation, different from other particle types (e.g., aged EC particles  
374 externally mixed with oxalate). It would have important implication for accurate modeling  
375 the formation and influence of oxalate in the atmosphere.

376

### 377 **Acknowledgement**

378 This work was supported by the National Key Research and Development Program of  
379 China (2017YFC0210104), the National Nature Science Foundation of China (No.  
380 91544101), and the Foundation for Leading Talents of the Guangdong Province Government.  
381 G.H. Zhang would like to thank the support from State Key Laboratory of Organic  
382 Geochemistry (SKLOG2016-A05).



---

### 383 References

384 Bi, X. H., Zhang, G. H., Li, L., Wang, X. M., Li, M., Sheng, G. Y., Fu, J. M., and Zhou,  
385 Z.: Mixing state of biomass burning particles by single particle aerosol mass spectrometer in  
386 the urban area of PRD, China, *Atmos. Environ.*, 45, 3447-3453,  
387 doi:10.1016/j.atmosenv.2011.03.034, 2011.

388 Bi, X. H., Lin, Q. H., Peng, L., Zhang, G. H., Wang, X. M., Brechtel, F. J., Chen, D. H.,  
389 Li, M., Peng, P. A., Sheng, G. Y., and Zhou, Z.: In situ detection of the chemistry of individual  
390 fog droplet residues in the Pearl River Delta region, China, *J. Geophys. Res.-Atmos.*, 121, 9105-  
391 9116, doi:10.1002/2016JD024886, 2016.

392 Carlton, A. G., Turpin, B. J., Lim, H. J., Altieri, K. E., and Seitzinger, S.: Link between  
393 isoprene and secondary organic aerosol (SOA): Pyruvic acid oxidation yields low volatility  
394 organic acids in clouds, *Geophys. Res. Lett.*, 33, L06822, doi:10.1029/2005gl025374, 2006.

395 Carlton, A. G., Turpin, B. J., Altieri, K. E., Seitzinger, S., Reff, A., Lim, H. J., and Ervens,  
396 B.: Atmospheric oxalic acid and SOA production from glyoxal: Results of aqueous  
397 photooxidation experiments, *Atmos. Environ.*, 41, 7588-7602,  
398 doi:10.1016/j.atmosenv.2007.05.035, 2007.

399 Cheng, C., Li, M., Chan, C. K., Tong, H., Chen, C., Chen, D., Wu, D., Li, L., Wu, C.,  
400 Cheng, P., Gao, W., Huang, Z., Li, X., Zhang, Z., Fu, Z., Bi, Y., and Zhou, Z.: Mixing state of  
401 oxalic acid containing particles in the rural area of Pearl River Delta, China: implications for  
402 the formation mechanism of oxalic acid, *Atmos. Chem. Phys.*, 17, 9519-9533, doi:10.5194/acp-  
403 17-9519-2017, 2017.

404 Crahan, K. K., Hegg, D., Covert, D. S., and Jonsson, H.: An exploration of aqueous oxalic  
405 acid production in the coastal marine atmosphere, *Atmos. Environ.*, 38, 3757-3764, 2004.

406 Cubison, M. J., Ortega, A. M., Hayes, P. L., Farmer, D. K., Day, D., Lechner, M. J., Brune,  
407 W. H., Apel, E., Diskin, G. S., Fisher, J. A., Fuelberg, H. E., Hecobian, A., Knapp, D. J.,  
408 Mikoviny, T., Riemer, D., Sachse, G. W., Sessions, W., Weber, R. J., Weinheimer, A. J.,  
409 Wisthaler, A., and Jimenez, J. L.: Effects of aging on organic aerosol from open biomass



- 
- 410 burning smoke in aircraft and laboratory studies, *Atmos. Chem. Phys.*, 11, 12049-12064,  
411 doi:10.5194/acp-11-12049-2011, 2011.
- 412 Dall'Osto, M., Harrison, R. M., Coe, H., and Williams, P.: Real-time secondary aerosol  
413 formation during a fog event in London, *Atmos. Chem. Phys.*, 9, 2459-2469, 2009.
- 414 Deshmukh, D. K., Kawamura, K., and Deb, M. K.: Dicarboxylic acids,  $\omega$ -oxocarboxylic  
415 acids,  $\alpha$ -dicarbonyls, WSOC, OC, EC, and inorganic ions in wintertime size-segregated  
416 aerosols from central India: Sources and formation processes, *Chemosphere*, 161, 27-42,  
417 doi:10.1016/j.chemosphere.2016.06.107, 2016.
- 418 Draxler, R. R., and Rolph, G. D.: HYSPLIT (HYbrid Single-Particle Lagrangian  
419 Integrated Trajectory) Model access via NOAA ARL READY Website  
420 (<http://ready.arl.noaa.gov/HYSPLIT.php>), NOAA Air Resources Laboratory, MD, Silver  
421 Spring, 2012.
- 422 Ervens, B., Feingold, G., Frost, G. J., and Kreidenweis, S. M.: A modeling study of  
423 aqueous production of dicarboxylic acids: 1. Chemical pathways and speciated organic mass  
424 production, *J. Geophys. Res.-Atmos.*, 109, 1265-1277, doi:10.1029/2003jd004387, 2004.
- 425 Ervens, B., Turpin, B. J., and Weber, R. J.: Secondary organic aerosol formation in cloud  
426 droplets and aqueous particles (aqSOA): a review of laboratory, field and model studies, *Atmos.*  
427 *Chem. Phys.*, 11, 11069-11102, doi:10.5194/acp-11-11069-2011, 2011.
- 428 Ervens, B., Sorooshian, A., Lim, Y. B., and Turpin, B. J.: Key parameters controlling OH-  
429 initiated formation of secondary organic aerosol in the aqueous phase (aqSOA), *J. Geophys.*  
430 *Res.-Atmos.*, 119, 3997-4016, doi:10.1002/2013JD021021, 2014.
- 431 Ervens, B.: Modeling the Processing of Aerosol and Trace Gases in Clouds and Fogs,  
432 *Chem. Rev.*, 115, 4157-4198, doi:10.1021/cr5005887, 2015.
- 433 Feng, J. L., Guo, Z. G., Zhang, T. R., Yao, X. H., Chan, C. K., and Fang, M.: Source and  
434 formation of secondary particulate matter in PM<sub>2.5</sub> in Asian continental outflow, *J. Geophys.*  
435 *Res.-Atmos.*, 117, 812-819, doi:10.1029/2011jd016400, 2012.



- 436 Furukawa, T., and Takahashi, Y.: Oxalate metal complexes in aerosol particles:  
437 implications for the hygroscopicity of oxalate-containing particles, *Atmos. Chem. Phys.*, 11,  
438 4289-4301, doi:10.5194/acp-11-4289-2011, 2011.
- 439 Gao, S., Hegg, D. A., Hobbs, P. V., Kirchstetter, T. W., Magi, B. I., and Sadilek, M.:  
440 Water-soluble organic components in aerosols associated with savanna fires in southern Africa:  
441 Identification, evolution, and distribution, *J. Geophys. Res.-Atmos.*, 108, 471-475, 2003.
- 442 Gilardoni, S., Massoli, P., Paglione, M., Giulianelli, L., Carbone, C., Rinaldi, M., Decesari,  
443 S., Sandrini, S., Costabile, F., Gobbi, G. P., Pietrogrande, M. C., Visentin, M., Scotto, F., Fuzzi,  
444 S., and Facchini, M. C.: Direct observation of aqueous secondary organic aerosol from biomass-  
445 burning emissions, *Proc. Natl. Acad. Sci. USA*, 113, 10013-10018, 2016.
- 446 Guo, T. F., Li, K., Zhu, Y. J., Gao, H. W., and Yao, X. H.: Concentration and size  
447 distribution of particulate oxalate in marine and coastal atmospheres - Implication for the  
448 increased importance of oxalate in nanometer atmospheric particles, *Atmos. Environ.*, 142, 19-  
449 31, 2016.
- 450 Hara, K., Osada, K., Matsunaga, K., Sakai, T., Iwasaka, Y., and Furuya, K.: Concentration  
451 trends and mixing states of particulate oxalate in Arctic boundary layer in winter/spring, *J.*  
452 *Geophys. Res.-Atmos.*, 107, AAC 12-11 - AAC 12-14, 2002.
- 453 Healy, R. M., Sciare, J., Poulain, L., Crippa, M., Wiedensohler, A., Prevot, A. S. H.,  
454 Baltensperger, U., Sarda-Esteve, R., McGuire, M. L., Jeong, C. H., McGillicuddy, E., O'Connor,  
455 I. P., Sodeau, J. R., Evans, G. J., and Wenger, J. C.: Quantitative determination of carbonaceous  
456 particle mixing state in Paris using single-particle mass spectrometer and aerosol mass  
457 spectrometer measurements, *Atmos. Chem. Phys.*, 13, 9479-9496, doi:10.5194/acp-13-9479-  
458 2013, 2013.
- 459 Herrmann, H., Schaefer, T., Tilgner, A., Styler, S. A., Weller, C., Teich, M., and Otto, T.:  
460 Tropospheric Aqueous-Phase Chemistry: Kinetics, Mechanisms, and Its Coupling to a  
461 Changing Gas Phase, *Chem. Rev.*, 115, 4259-4334, doi:10.1021/cr500447k, 2015.
- 462 Ho, K. F., Lee, S. C., Ho, S. S. H., Kawamura, K., Tachibana, E., Cheng, Y., and Zhu, T.:  
463 Dicarboxylic acids, ketocarboxylic acids, alpha-dicarbonyls, fatty acids, and benzoic acid in



464 urban aerosols collected during the 2006 Campaign of Air Quality Research in Beijing  
465 (CAREBeijing-2006), *J. Geophys. Res.-Atmos.*, 115, D19312, 2010.

466 Huang, X. F., Yu, J. Z., He, L. Y., and Yuan, Z. B.: Water-soluble organic carbon and  
467 oxalate in aerosols at a coastal urban site in China: Size distribution characteristics, sources,  
468 and formation mechanisms, *J. Geophys. Res.-Atmos.*, 111, D22212,  
469 doi:10.1029/2006jd007408, 2006.

470 Huo, J., Lu, X., Wang, X., Chen, H., Ye, X., Gao, S., Gross, D. S., Chen, J., and Yang, X.:  
471 Online single particle analysis of chemical composition and mixing state of crop straw burning  
472 particles: from laboratory study to field measurement, *Frontiers of Environmental Science &*  
473 *Engineering*, 10, 244-252, doi:10.1007/s11783-015-0768-z, 2016.

474 Ito, A., and Shi, Z.: Delivery of anthropogenic bioavailable iron from mineral dust and  
475 combustion aerosols to the ocean, *Atmos. Chem. Phys.*, 16, 85-99, doi:10.5194/acp-16-85-2016,  
476 2016.

477 Jeong, C. H., McGuire, M. L., Godri, K. J., Slowik, J. G., Rehbein, P. J. G., and Evans, G.  
478 J.: Quantification of aerosol chemical composition using continuous single particle  
479 measurements, *Atmos. Chem. Phys.*, 11, 7027-7044, doi:10.5194/acp-11-7027-2011, 2011.

480 Johnson, M. S., and Meskhidze, N.: Atmospheric dissolved iron deposition to the global  
481 oceans: effects of oxalate-promoted Fe dissolution, photochemical redox cycling, and dust  
482 mineralogy, *Geoscientific Model Development*, 6, 1137-1155, doi:10.5194/gmd-6-1137-2013,  
483 2013.

484 Kawamura, K., Tachibana, E., Okuzawa, K., Aggarwal, S. G., Kanaya, Y., and Wang, Z.  
485 F.: High abundances of water-soluble dicarboxylic acids, ketocarboxylic acids and alpha-  
486 dicarbonyls in the mountaintop aerosols over the North China Plain during wheat burning  
487 season, *Atmos. Chem. Phys.*, 13, 8285-8302, 2013.

488 Kawamura, K., and Bikkina, S.: A review of dicarboxylic acids and related compounds in  
489 atmospheric aerosols: Molecular distributions, sources and transformation, *Atmos. Res.*, 170,  
490 140-160, 2016.





- 
- 491 Kundu, S., Kawamura, K., Andreae, T. W., Hoffer, A., and Andreae, M. O.: Molecular  
492 distributions of dicarboxylic acids, ketocarboxylic acids and alpha-dicarbonyls in biomass  
493 burning aerosols: implications for photochemical production and degradation in smoke layers,  
494 Atmos. Chem. Phys., 10, 2209-2225, 2010.
- 495 Laongsri, B., and Harrison, R. M.: Atmospheric behaviour of particulate oxalate at UK  
496 urban background and rural sites, Atmos. Environ., 71, 319-326, 2013.
- 497 Li, L., Huang, Z. X., Dong, J. G., Li, M., Gao, W., Nian, H. Q., Fu, Z., Zhang, G. H., Bi,  
498 X. H., Cheng, P., and Zhou, Z.: Real time bipolar time-of-flight mass spectrometer for analyzing  
499 single aerosol particles, Intl. J. Mass. Spectrom., 303, 118-124, doi:10.1016/j.ijms.2011.01.017,  
500 2011a.
- 501 Li, W. J., Li, P. R., Sun, G. D., Zhou, S. Z., Yuan, Q., and Wang, W. X.: Cloud residues  
502 and interstitial aerosols from non-precipitating clouds over an industrial and urban area in  
503 northern China, Atmos. Environ., 45, 2488-2495, doi:10.1016/j.atmosenv.2011.02.044, 2011b.
- 504 Lin, Q., Zhang, G., Peng, L., Bi, X., Wang, X., Brechtel, F. J., Li, M., Chen, D., Peng, P.,  
505 Sheng, G., and Zhou, Z.: In situ chemical composition measurement of individual cloud residue  
506 particles at a mountain site, southern China, Atmos. Chem. Phys., 17, 8473-8488,  
507 doi:10.5194/acp-17-8473-2017, 2017.
- 508 McNeill, V. F.: Aqueous Organic Chemistry in the Atmosphere: Sources and Chemical  
509 Processing of Organic Aerosols, Environ. Sci. Technol., 49, 1237-1244,  
510 doi:10.1021/es5043707, 2015.
- 511 Meng, J. J., Wang, G. H., Li, J. J., Cheng, C. L., and Cao, J. J.: Atmospheric oxalic acid  
512 and related secondary organic aerosols in Qinghai Lake, a continental background site in Tibet  
513 Plateau, Atmos. Environ., 79, 582-589, 2013.
- 514 Meng, J. J., Wang, G. H., Li, J. J., Cheng, C. L., Ren, Y. Q., Huang, Y., Cheng, Y. T., Cao,  
515 J. J., and Zhang, T.: Seasonal characteristics of oxalic acid and related SOA in the free  
516 troposphere of Mt. Hua, central China: Implications for sources and formation mechanisms, Sci.  
517 Total. Environ., 493, 1088-1097, 2014.



- 518 Miyazaki, Y., Aggarwal, S. G., Singh, K., Gupta, P. K., and Kawamura, K.: Dicarboxylic  
519 acids and water-soluble organic carbon in aerosols in New Delhi, India, in winter:  
520 Characteristics and formation processes, *J. Geophys. Res.-Atmos.*, 114, D19206, 2009.
- 521 Mochida, M., Umemoto, N., Kawamura, K., Lim, H. J., and Turpin, B. J.: Bimodal size  
522 distributions of various organic acids and fatty acids in the marine atmosphere: Influence of  
523 anthropogenic aerosols, Asian dusts, and sea spray off the coast of East Asia, *J. Geophys. Res.-*  
524 *Atmos.*, 112, 229-238, 2007.
- 525 Myriokefalitakis, S., Tsigaridis, K., Mihalopoulos, N., Sciare, J., Nenes, A., Kawamura,  
526 K., Segers, A., and Kanakidou, M.: In-cloud oxalate formation in the global troposphere: a 3-  
527 D modeling study, *Atmos. Chem. Phys.*, 11, 5761-5782, doi:10.5194/acp-11-5761-2011, 2011.
- 528 Nguyen, T. B., Coggon, M. M., Flagan, R. C., and Seinfeld, J. H.: Reactive Uptake and  
529 Photo-Fenton Oxidation of Glycolaldehyde in Aerosol Liquid Water, *Environ. Sci. Technol.*,  
530 47, 4307-4316, doi:10.1021/es400538j, 2013.
- 531 Paglione, M., Saarikoski, S., Carbone, S., Hillamo, R., Facchini, M. C., Finessi, E.,  
532 Giulianelli, L., Carbone, C., Fuzzi, S., Moretti, F., Tagliavini, E., Swietlicki, E., Stenstrom, K.  
533 E., Prevot, A. S. H., Massoli, P., Canaragatna, M., Worsnop, D., and Decesari, S.: Primary and  
534 secondary biomass burning aerosols determined by proton nuclear magnetic resonance (H-1-  
535 NMR) spectroscopy during the 2008 EUCAARI campaign in the Po Valley (Italy), *Atmos.*  
536 *Chem. Phys.*, 14, 5089-5110, doi:10.5194/acp-14-5089-2014, 2014.
- 537 Pratt, K. A., Heymsfield, A. J., Twohy, C. H., Murphy, S. M., DeMott, P. J., Hudson, J.  
538 G., Subramanian, R., Wang, Z. E., Seinfeld, J. H., and Prather, K. A.: In Situ Chemical  
539 Characterization of Aged Biomass-Burning Aerosols Impacting Cold Wave Clouds, *J. Atmos.*  
540 *Sci.*, 67, 2451-2468, doi:10.1175/2010JAS3330.1, 2010.
- 541 Rehbein, P. J. G., Jeong, C. H., McGuire, M. L., Yao, X. H., Corbin, J. C., and Evans, G.  
542 J.: Cloud and Fog Processing Enhanced Gas-to-Particle Partitioning of Trimethylamine,  
543 *Environ. Sci. Technol.*, 45, 4346-4352, doi:10.1021/es1042113, 2011.



- 
- 544 Reid, J. S., Koppmann, R., Eck, T. F., and Eleuterio, D. P.: A review of biomass burning  
545 emissions part II: intensive physical properties of biomass burning particles, Atmos. Chem.  
546 Phys., 5, 799-825, 2005.
- 547 Schroder, J. C., Hanna, S. J., Modini, R. L., Corrigan, A. L., Kreidenwies, S. M.,  
548 Macdonald, A. M., Noone, K. J., Russell, L. M., Leaitch, W. R., and Bertram, A. K.: Size-  
549 resolved observations of refractory black carbon particles in cloud droplets at a marine  
550 boundary layer site, Atmos. Chem. Phys., 15, 1367-1383, doi:10.5194/acp-15-1367-2015, 2015.
- 551 Shingler, T., Dey, S., Sorooshian, A., Brechtel, F. J., Wang, Z., Metcalf, A., Coggon, M.,  
552 Mulmenstadt, J., Russell, L. M., Jonsson, H. H., and Seinfeld, J. H.: Characterisation and  
553 airborne deployment of a new counterflow virtual impactor inlet, Atmos. Meas. Tech., 5, 1259-  
554 1269, doi:10.5194/amt-5-1259-2012, 2012.
- 555 Silva, P. J., Liu, D. Y., Noble, C. A., and Prather, K. A.: Size and chemical characterization  
556 of individual particles resulting from biomass burning of local Southern California species,  
557 Environ. Sci. Technol., 33, 3068-3076, 1999.
- 558 Song, X. H., Hopke, P. K., Fergenson, D. P., and Prather, K. A.: Classification of single  
559 particles analyzed by ATOFMS using an artificial neural network, ART-2A, Anal. Chem., 71,  
560 860-865, 1999.
- 561 Sorooshian, A., Varutbangkul, V., Brechtel, F. J., Ervens, B., Feingold, G., Bahreini, R.,  
562 Murphy, S. M., Holloway, J. S., Atlas, E. L., Buzorius, G., Jonsson, H., Flagan, R. C., and  
563 Seinfeld, J. H.: Oxalic acid in clear and cloudy atmospheres: Analysis of data from International  
564 Consortium for Atmospheric Research on Transport and Transformation 2004, J. Geophys.  
565 Res.-Atmos., 111, 23-45, doi:10.1029/2005jd006880, 2006.
- 566 Sorooshian, A., Lu, M. L., Brechtel, F. J., Jonsson, H., Feingold, G., Flagan, R. C., and  
567 Seinfeld, J. H.: On the source of organic acid aerosol layers above clouds, Environ. Sci.  
568 Technol., 41, 4647-4654, 2007a.
- 569 Sorooshian, A., Ng, N. L., Chan, A. W. H., Feingold, G., Flagan, R. C., and Seinfeld, J.  
570 H.: Particulate organic acids and overall water-soluble aerosol composition measurements from



- 
- 571 the 2006 Gulf of Mexico Atmospheric Composition and Climate Study (GoMACCS), J.  
572 Geophys. Res.-Atmos., 112, 125-138, doi:10.1029/2007jd008537, 2007b.
- 573 Sorooshian, A., Wang, Z., Coggon, M. M., Jonsson, H. H., and Ervens, B.: Observations  
574 of Sharp Oxalate Reductions in Stratocumulus Clouds at Variable Altitudes: Organic Acid and  
575 Metal Measurements During the 2011 E-PEACE Campaign, Environ. Sci. Technol., 47, 7747-  
576 7756, doi:10.1021/es4012383, 2013.
- 577 Sullivan, R. C., Guazzotti, S. A., Sodeman, D. A., and Prather, K. A.: Direct observations  
578 of the atmospheric processing of Asian mineral dust, Atmos. Chem. Phys., 7, 1213-1236,  
579 doi:10.5194/acp-7-1213-2007, 2007.
- 580 Sullivan, R. C., and Prather, K. A.: Investigations of the diurnal cycle and mixing state of  
581 oxalic acid in individual particles in Asian aerosol outflow, Environ. Sci. Technol., 41, 8062-  
582 8069, 2007.
- 583 Wonaschuetz, A., Sorooshian, A., Ervens, B., Chuang, P. Y., Feingold, G., Murphy, S. M.,  
584 de Gouw, J., Warneke, C., and Jonsson, H. H.: Aerosol and gas re-distribution by shallow  
585 cumulus clouds: An investigation using airborne measurements, J. Geophys. Res.-Atmos., 117,  
586 202, doi:10.1029/2012jd018089, 2012.
- 587 Yang, F., Chen, H., Wang, X. N., Yang, X., Du, J. F., and Chen, J. M.: Single particle  
588 mass spectrometry of oxalic acid in ambient aerosols in Shanghai: Mixing state and formation  
589 mechanism, Atmos. Environ., 43, 3876-3882, 2009.
- 590 Yang, F., Gu, Z. P., Feng, J. L., Liu, X. H., and Yao, X. H.: Biogenic and anthropogenic  
591 sources of oxalate in PM<sub>2.5</sub> in a mega city, Shanghai, Atmos. Res., 138, 356-363,  
592 doi:10.1016/j.atmosres.2013.12.006, 2014.
- 593 Yu, J. Z., Huang, X. F., Xu, J. H., and Hu, M.: When aerosol sulfate goes up, so does  
594 oxalate: Implication for the formation mechanisms of oxalate, Environ. Sci. Technol., 39, 128-  
595 133, doi:10.1021/Es049559f, 2005.
- 596 Zauscher, M. D., Wang, Y., Moore, M. J. K., Gaston, C. J., and Prather, K. A.: Air Quality  
597 Impact and Physicochemical Aging of Biomass Burning Aerosols during the 2007 San Diego  
598 Wildfires, Environ. Sci. Technol., 47, 7633-7643, doi:10.1021/es4004137, 2013.



- 
- 599           Zhang, G. H., Bi, X. H., Chan, L. Y., Li, L., Wang, X. M., Feng, J. L., Sheng, G. Y., Fu,  
600 J. M., Li, M., and Zhou, Z.: Enhanced trimethylamine-containing particles during fog events  
601 detected by single particle aerosol mass spectrometry in urban Guangzhou, China, *Atmos.*  
602 *Environ.*, 55, 121-126, doi:10.1016/j.atmosenv.2012.03.038, 2012.
- 603           Zhang, Y. L., Kawamura, K., Fu, P. Q., Boreddy, S. K. R., Watanabe, T., Hatakeyama, S.,  
604 Takami, A., and Wang, W.: Aircraft observations of water-soluble dicarboxylic acids in the  
605 aerosols over China, *Atmos. Chem. Phys.*, 16, 6407-6419, doi:10.5194/acp-16-6407-2016,  
606 2016.
- 607           Zhou, S., Collier, S., Jaffè, D. A., Briggs, N. L., Hee, J., Sedlacek Iii, A. J., Kleinman, L.,  
608 Onasch, T. B., and Zhang, Q.: Regional influence of wildfires on aerosol chemistry in the  
609 western US and insights into atmospheric aging of biomass burning organic aerosol, *Atmos.*  
610 *Chem. Phys.*, 17, 2477-2493, doi:10.5194/acp-17-2477-2017, 2017.
- 611           Zhou, Y., Huang, X. H., Bian, Q., Griffith, S. M., Louie, P. K. K., and Yu, J. Z.: Sources  
612 and atmospheric processes impacting oxalate at a suburban coastal site in Hong Kong: Insights  
613 inferred from 1 year hourly measurements, *J. Geophys. Res.-Atmos.*, 120, 9772-9788,  
614 doi:10.1002/2015jd023531, 2015.
- 615



616 **Tables**

617 **Table 1. The number and number fraction of oxalate-containing particles in**

618 **the all the detected cloud-free, RES, and INT particles.**

	Cloud-free	Cloud RES	Cloud INT
Num. of all the detected particles	48835	23616	1063
Num. of oxalate-containing particles	2442	3410	142
Nf. of oxalate-containing particles	$5.0 \pm 0.1\%$	$14.4 \pm 0.2\%$	$13.4 \pm 1.1\%$
Nf. of oxalate-containing particles classified as aged biomass burning particles	$76.3 \pm 1.8\%$	$70.0 \pm 1.4\%$	$71.8 \pm 7.1\%$

619



620 **Figure caption**

621 Fig. 1. (a) Temporal variation (in one-hour resolution) of Nfs of the oxalate-  
622 containing particles, and box-and-whisker plots of (b) the Nf of oxalate-containing  
623 particles, and (c) the relative peak area (RPA) of oxalate, separated for the cloud-free,  
624 cloud RES, and cloud INT particles. In a box and whisker plot, the lower, median and  
625 upper line of the box denote the 25, 50, and 75 percentiles, respectively; the lower and  
626 upper edges of the whisker denote the 10 and 90 percentiles, respectively. Red triangles  
627 refer to the arithmetical mean values of the Nfs and RPAs shown in (b) and (c).

628 Fig. 2. Size dependent Nfs of oxalate-containing particles relative to all the  
629 detected cloud-free, cloud RES, and cloud INT particles, respectively.

630 Fig. 3. Number fractions of the major ion peaks in oxalate-containing and all the  
631 detected particles, respectively.

632 Fig. 4. Number fractions of the single particle types for oxalate-containing and all  
633 the detected particles, respectively.

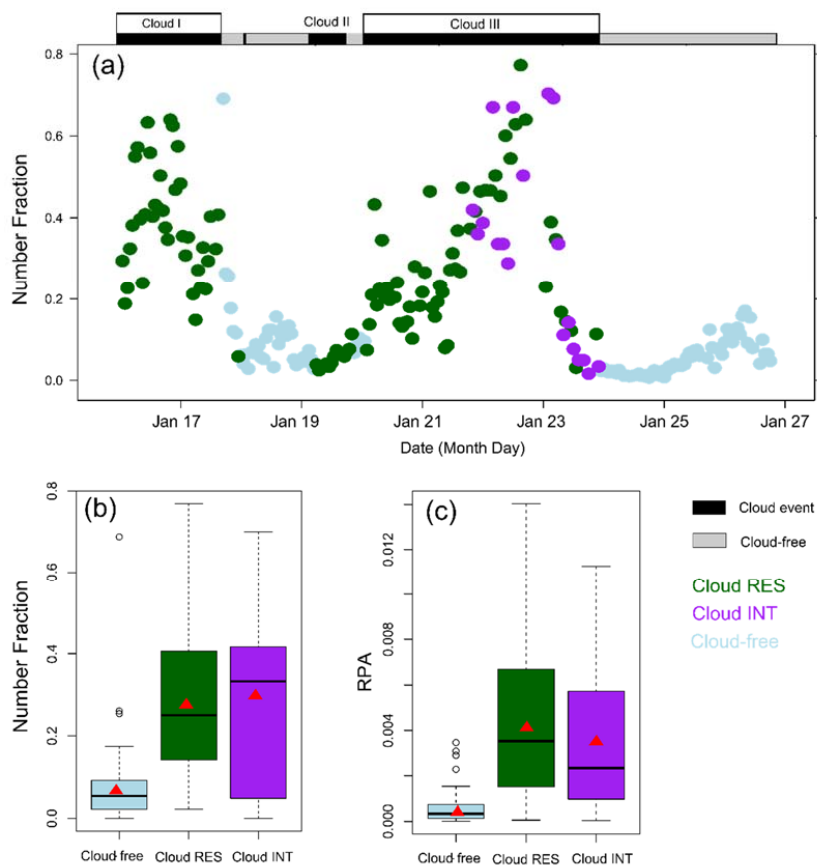
634 Fig. 5. Correlation analysis between (a) the Nfs and (b) The RPAs of the oxalate-  
635 containing and glyoxylate-containing particles, separated for the cloud-free, cloud RES,  
636 and cloud INT particles, respectively.

637 Fig. 6. The relative distributions of the peak areas of oxalate, glyoxylate, and the  
638 OAs for (a) the individual cloud-free and (b) the cloud RES and cloud INT oxalate-  
639 containing particles. The peak areas of the OAs were summed from those of the  
640 individual OAs. The coloration indicates the RPA of oxalate.



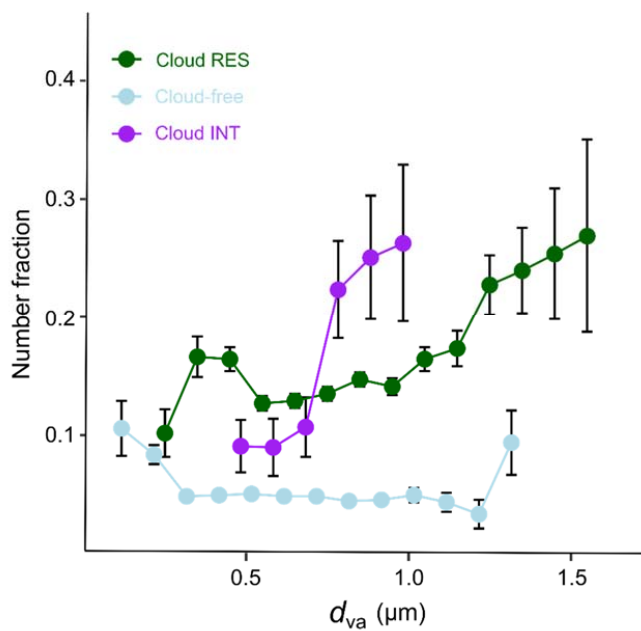
641 Fig. 7. Box and whisker plots of the variations of  $N_f$ s for the K-rich, oxalate-  
642 containing, and glyoxylate-containing particles during the cloud events, respectively.





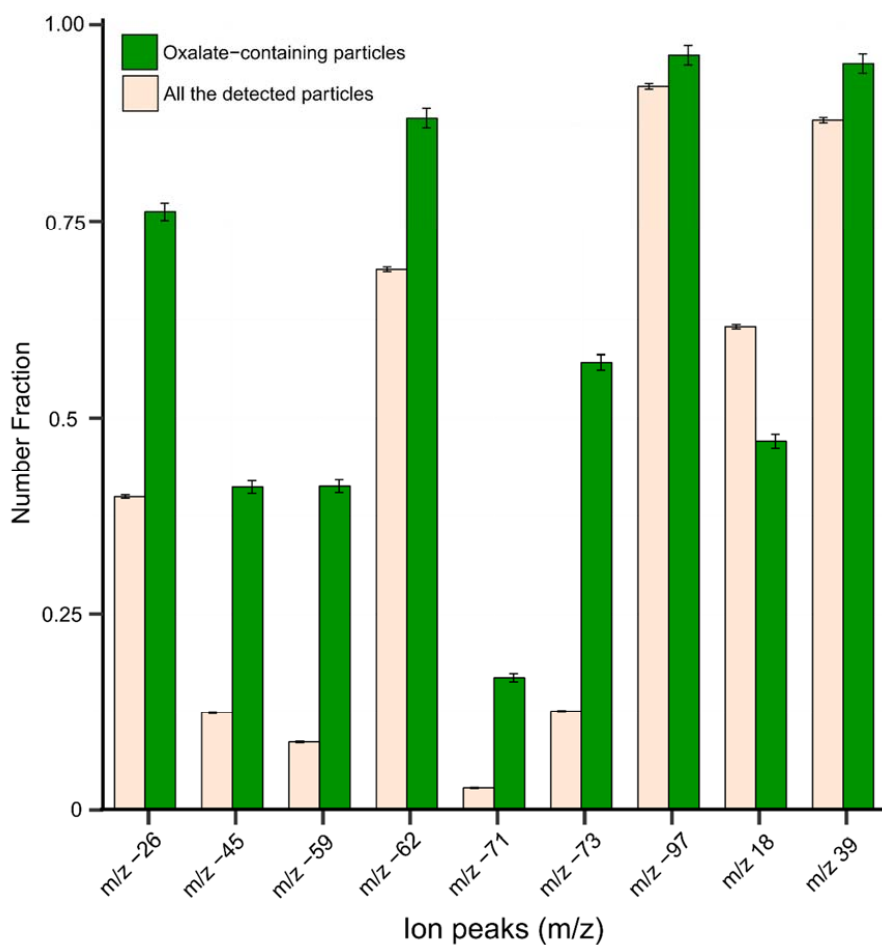
643

644 Fig. 1.



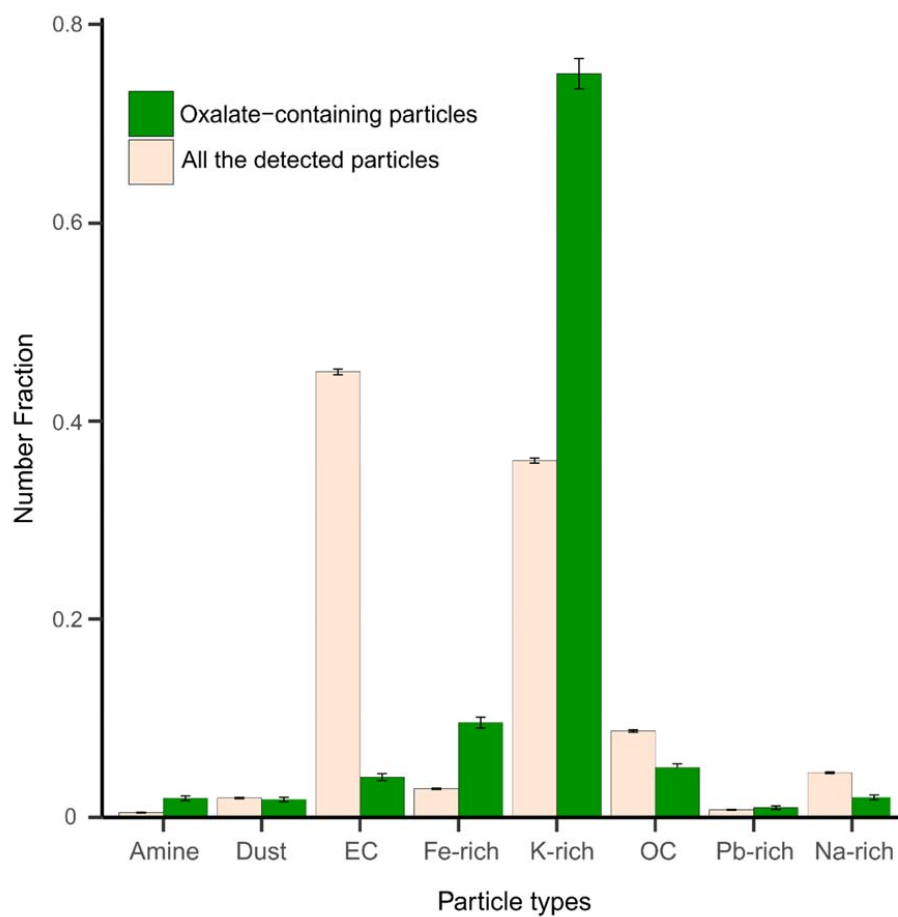
645

646 Fig. 2.



647

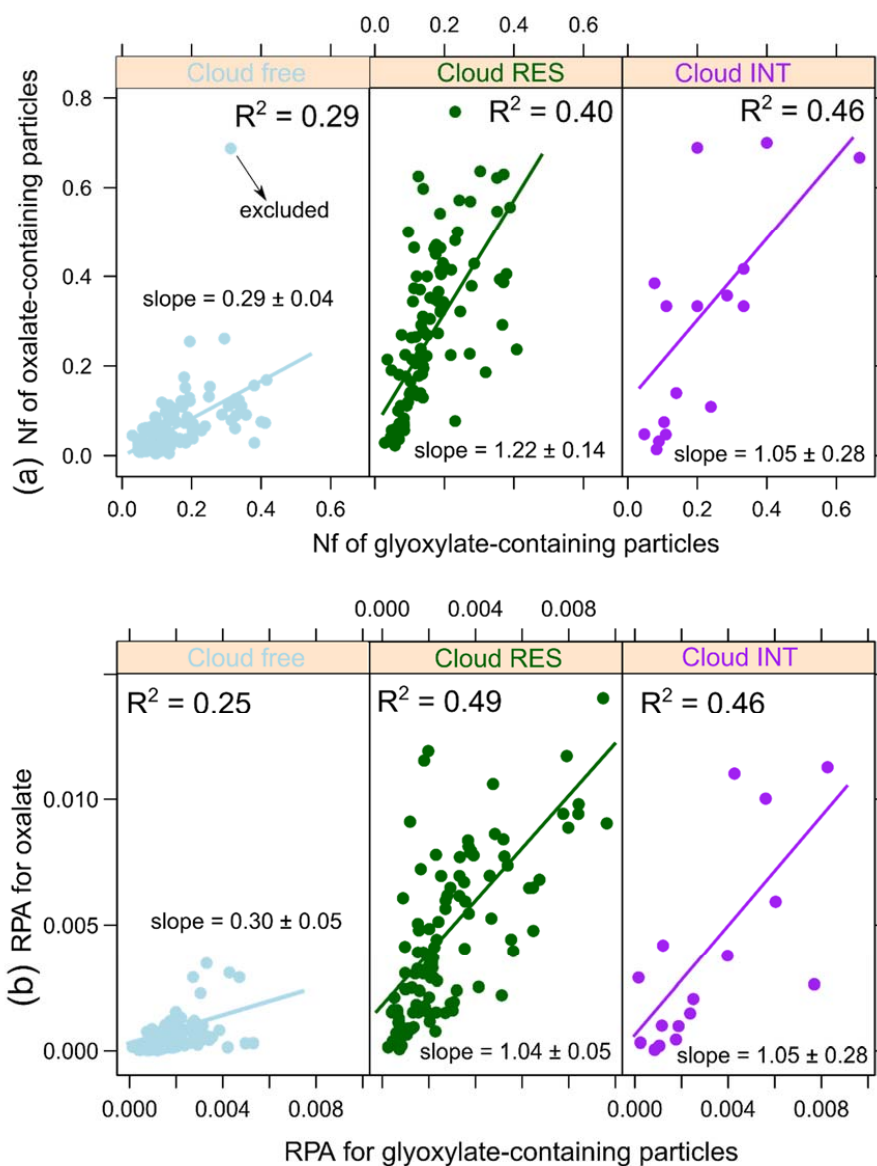
648 **Fig. 3.**



649

650

**Fig. 4.**

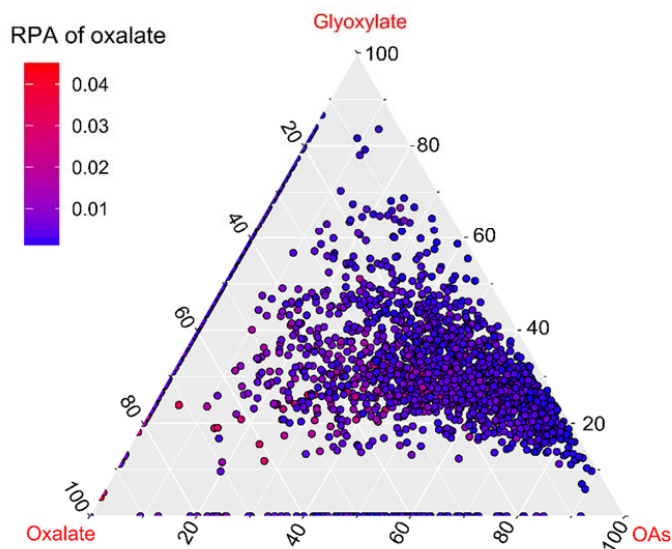


651

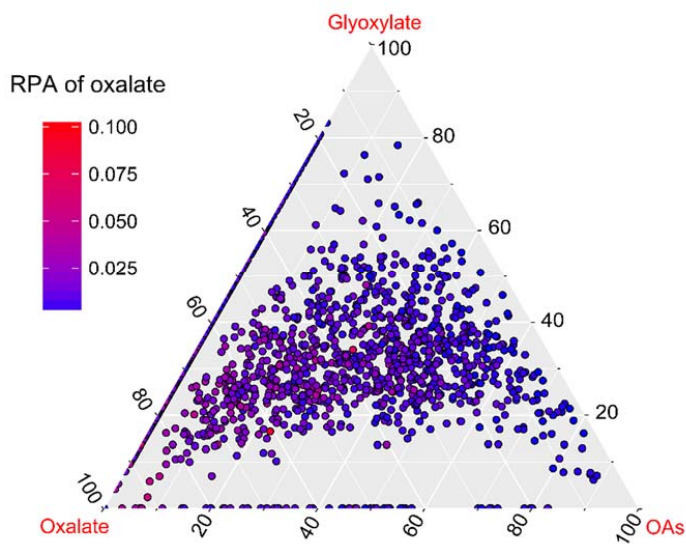
652 **Fig. 5.**



(a) cloud-free oxalate-containing particles



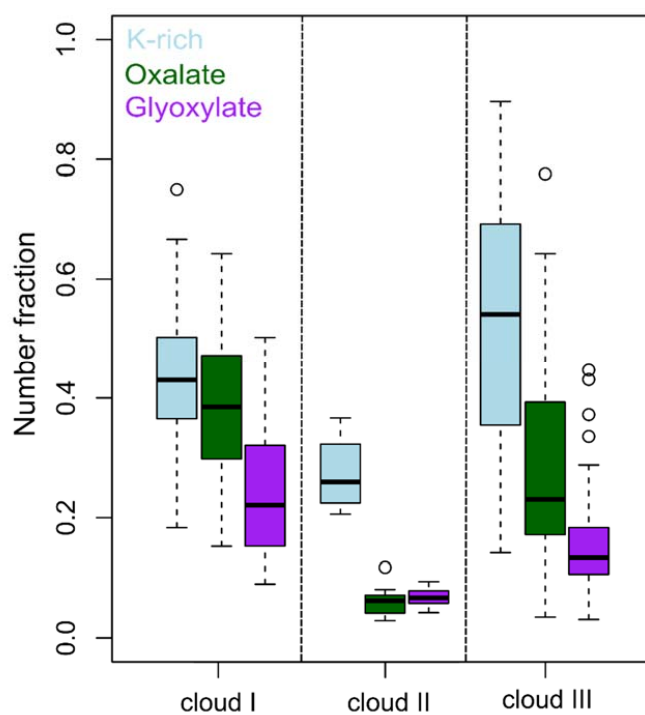
(b) cloud RES and INT oxalate-containing particles



653

654

**Fig. 6.**



655

656 **Fig. 7.**